Computational Materials Science 202 (2022) 110962

Contents lists available at ScienceDirect

Computational Materials Science

journal homepage: www.elsevier.com/locate/commatsci

The N-body interatomic potential for molecular dynamics simulations of diffusion in tungsten

V.N. Maksimenko [a,b], A.G. Lipnitskii [a,b], A.I. Kartamyshev [c,d,*], D.O. Poletaev [a], Yu. R. Kolobov [b]

[a] The Center of Nanostructured Materials and Nanotechnologies, Belgorod State University, Belgorod, Russian Federation
[b] Institute of Problems of Chemical Physics (IPCP), Russian Academy of Sciences, Chernogolovka, Moscow, Russia
[c] Division of Computational Physics, Institute for Computational Science, Ton Duc Thang University, Ho Chi Minh City, Viet Nam
[d] Faculty of Electrical & Electronics Engineering, Ton Duc Thang University, Ho Chi Minh City, Viet Nam

ARTICLE INFO

Keywords:
Interatomic potentials
Molecular dynamics
Diffusion
Tungsten

ABSTRACT

Tungsten, as the most refractory metal, is applied in fusion reactor in parts subjected to high temperatures and strong neutron irradiation. These factors lead to intense diffusion processes causing degradation of the material. Experimental investigations under such conditions are usually highly complicated and cannot provide a comprehensive understanding of the occurring phenomena. Therefore, their combination with theoretical approaches is required. One of the most robust approaches to simulate diffusion processes is molecular dynamics simulations based on classical interatomic potentials. It allows modeling relatively large samples consisting of several grains, grain boundaries, dislocations, and other types of defects for a reasonable computational time. The reliable simulations of the diffusion process require interatomic potentials satisfying the following criteria: prediction of melting point and thermal expansion as close as possible to the experimental values because the diffusion coefficient strongly depends on the homologous temperature and size factor. In the present paper, we present the new interatomic potential for tungsten, developed within the N-body approach, which reproduces the experimental value of melting temperature (3695 K) and thermal expansion at temperatures up to a melting point. The calculated diffusion coefficient demonstrates adequate agreement with experimental results. The constructed potential is applicable for simulation of processes involving diffusion, one of which is the irradiation damage.

1. Introduction

Tungsten is one of the most refractory metals and is actively used in modern materials as a base for metallic materials employed at high operating temperatures. One of the possible applications of tungsten and its alloys is fusion reactors, in which they will be subjected to significant neutron irradiation leading to the degradation of the microstructure due to the diffusion processes caused by collision cascades [1]. The diffusivity significantly increases at elevated temperatures. Experimental investigations at such temperatures will encounter natural complications. Therefore their combination with theoretical approaches is required for a comprehensive understanding of such phenomena.

Molecular dynamics (MD) simulation is widely used for the simulation of the diffusion processes at elevated temperatures [2–5]. The interatomic potentials representing the dependence of the potential energy of the system of atoms on their coordinates are the key parts of this method. The calculation of diffusion coefficients imposes limitations on the quality of the interatomic potentials. Accurate reproduction of diffusion properties requires correct description of structural and elastic properties of ideal lattice, energies of point defects along with the accurate prediction of the melting point. The correct reproduce of the melting point will allow comparing the calculated diffusivities and any other properties with ones measured in the experiment at the same temperature since the homologous temperatures, which is equal to T/T_m (T_m - melting temperature), will coincide in both cases [6]. Thermal expansion is another crucial quantity for the reliable simulations of the diffusion processes. It is associated with the strong dependence of the defects properties, particularly vacancies and interstitial atoms, on size factor.

The proper prediction of defects' local surrounding is necessary for the accurate description of their migration, which represents the diffusion process, which, in turn, requires inclusion of angular dependency into the interatomic potentials. There are several approaches of the interatomic potentials' development, which employ the angular dependence. Among them we can mention the modified embedded atom method (MEAM) [7] and N-body approach [8–10],

* Corresponding author at: Institute for Computational Science, Ton Duc Thang University, Ho Chi Minh City, Viet Nam.
E-mail address: kartamyshevandrey@tdtu.edu.vn (A.I. Kartamyshev).

https://doi.org/10.1016/j.commatsci.2021.110962
Received 29 June 2021; Received in revised form 2 October 2021; Accepted 7 October 2021
Available online 1 November 2021

There are several interatomic potentials developed for tungsten [2, 11–13]. The most recent one was developed using the Gaussian approximation potential (GAP) framework [11]. The potential was constructed for the investigation of radiation damage; it predicts short-range many-body cascade dynamics and provides a good description of the liquid phase. Furthermore, the potential accurately reproduces surface properties and the energetics of vacancy and self-interstitial clusters. However, this potential still underestimates melting point and vacancy formation energy. The potential [12], also developed within the GAP framework, reproduces properties of various defects, such as surfaces, dislocations, and vacancies. However, it does not contain information about the prediction of melting and thermal properties, which are important for accurate diffusion simulations. The Finnis–Sinclair (FS) potential [13] correctly predicts vacancy formation energy and surface energy while not providing information about the melting temperature and self-diffusion. Chen et al. [2] constructed another FS potential for the investigation of the radiation defects in tungsten. It describes monovacancy and surface properties in agreement with known data. Meanwhile, it significantly overestimates the melting temperature (~900K) and deviates from the experiment in predicting thermal expansion at high temperatures.

In the present work, we employ the N-body method [8], which demonstrated its suitability for the description of atomic systems with metallic and covalent bonding types. This method was effectively used to construct interatomic potentials with a high predictive accuracy of the above-mentioned thermal properties important for the calculation of the diffusion coefficients including the potentials for pure metals (V, Ti) and alloys (Ti–V) [8,14–18]. Recently, we successfully exploited the N-body method to develop interatomic potentials applicable for the quantitative simulation of diffusion properties in vanadium-chromium system[19]. We fitted the present N-body potential not only to the theoretical data but also to the set of experimentally measured properties to increase its transferability and to obtain the agreement with the experiment as close as possible.

2. Interatomic potential for W

The n-body method of constructing potentials used in this work represents the potential energy of the E_{pot} of a system of N atoms in the form of contributions of pair interactions, three- and many-body interactions [8]

$$E_{tot} = \sum_{i<j}^{N} \Phi(R_{ji}) + \sum_{i}^{N} \sum_{k<j\neq i}^{N} \sum_{p,q}^{n_3} g^{pq}(cos(\theta_{jik})) f^{p}(R_{ji}) f^{q}(R_{ki}) + + \sum_{i}^{N} F(\bar{\rho}_i), \quad (1)$$

where

$$\bar{\rho}_i = \sum_{j\neq i} \rho(R_{ji}). \quad (2)$$

Here, R_{ji} - is the distance between atoms j and i, θ_{jik} - is the angle interatomic bonds ji and ki. The functions of a single variable $\Phi(R_{ji})$, $f^{p}(R_{ji})$, $g^{pq}(cos(\theta_{jik}))$, $F(\bar{\rho}_i)$, and $\rho(R_{ji})$ in relations (1) and (2) are potential functions defined by cubic splines. The values of the potential functions in the spline nodes are the optimized parameters. For small interatomic distances $R_{ji} < R_{ZBL}$, the pair potential $\Phi(R_{ji})$ is represented by Ziegler–Biersack–Littmark (ZBL) form [20]. The parameters are optimized by minimization of a target function to describe a database containing both experimental and theoretical information by the method of model temperature annealing in the parameter space (for more details, see Section 3.2 in [8]).

2.1. Optimization of the potential parameters

The *experimental* target values included the bcc tungsten lattice constant a_0, the sublimation energy E_{coh}, the elastic moduli C_{11}, C_{12}, C_{44}, and the equation of state $P(V)$.

The *theoretical* part of the fitting database consists of the results of DFT calculations. We employed the Vienna ab initio simulation package (VASP) [21] with pseudopotentials based on projector-augmented wave (PAW) [22] method for treatment of core and valence electrons. The exchange correlation energy was described by the generalized gradient approximation (GGA) using the PBE functional [23]. The calculations were carried out with a plane-wave cutoff energy of 600 eV and Γ-centered k-point meshes with linear density corresponding to one in the set of k-points for a bcc cubic cell containing two atoms (30 × 30 × 30). The integration over the Brillouin zone was made employing the Methfessel–Paxton smearing method [24] with 0.3 eV smearing width. The noted parameters of the DFT calculations provided the accuracy of the total energy ~ 0.1 meV/atom.

The DFT database consists of atomic energies and volumes of model systems (hcp, fcc, C32, A15, simple hexagonal and simple cubic). In addition, it includes energies and atomic forces for two bcc supercells, each with 128 atoms. In the first superlattice, one atom was shifted along the direction ⟨100⟩ from the equilibrium position by 0.05 Å. The second superlattice was obtained after the DFT molecular dynamics at a temperature of 1850 K. The selected set of DFT values reflects typical lattices for metals and represents a large set of atomic configurations with different distances between atoms and angles between bonds. All energies were used relative to one of the equilibrium bcc lattice. To overcome the discrepancy between the interatomic DFT distances and the experimental value of the equilibrium parameter of the bcc lattice of W, we scaled the interatomic distances in the model lattices. The scaling factor was chosen as the ratio of the experimental value, which was the target value, and the DFT equilibrium parameter of the bcc lattice of W at 0 K.

As a result of the optimization, about 40 potentials were constructed for W, from which one was selected with the closest to the experiment melting point's value (will be referred as POT_W hereinafter). Table A.1 in Appendix A lists arguments and values of the potential functions comprising the POT_W potential.

Fig. 1 illustrates the potential functions of the POT_W potential in graphical form. They have smooth dependencies on the arguments, which indicates that there is no overflow in the number of optimized parameters with the used base of target values.

2.2. Quality of fitting

Fig. 2 depicts the results of fitting of the atomic energies for a set of ideal crystal lattices of W. It shows that the energy values calculated using POT_W for all the considered model lattices are in good agreement with the results of DFT calculations. It is worthy to mention that the POT_W potential correctly reproduces the DFT sequence of energies from the lowest (bcc) to the highest (simple cubic). The maximum deviation is obtained for a simple hexagonal lattice and is 17%, which is insignificant due to its high energy (~ 1.0 eV) relative to the equilibrium bcc one. Thus, the POT_W potential sets the equilibrium bcc lattice W as the most energy favorable one.

The quality of the fitting of the experimental equation of state $P(V/V_0)$ is illustrated in Fig. 3. The perfect agreement is observed for the whole range of pressures considered in the experiment.

Table 1 presents the main characteristics of bcc tungsten used in the fitting of the POT_W potential in comparison with experimental and DFT values as well as the data obtained employing the newly constructed potential for W by the GAP method [11].

It demonstrates a quantitative agreement with the target experimental values of the sublimation energy, the lattice parameter, and the elastic moduli of the bcc lattice, and a qualitative with the data of

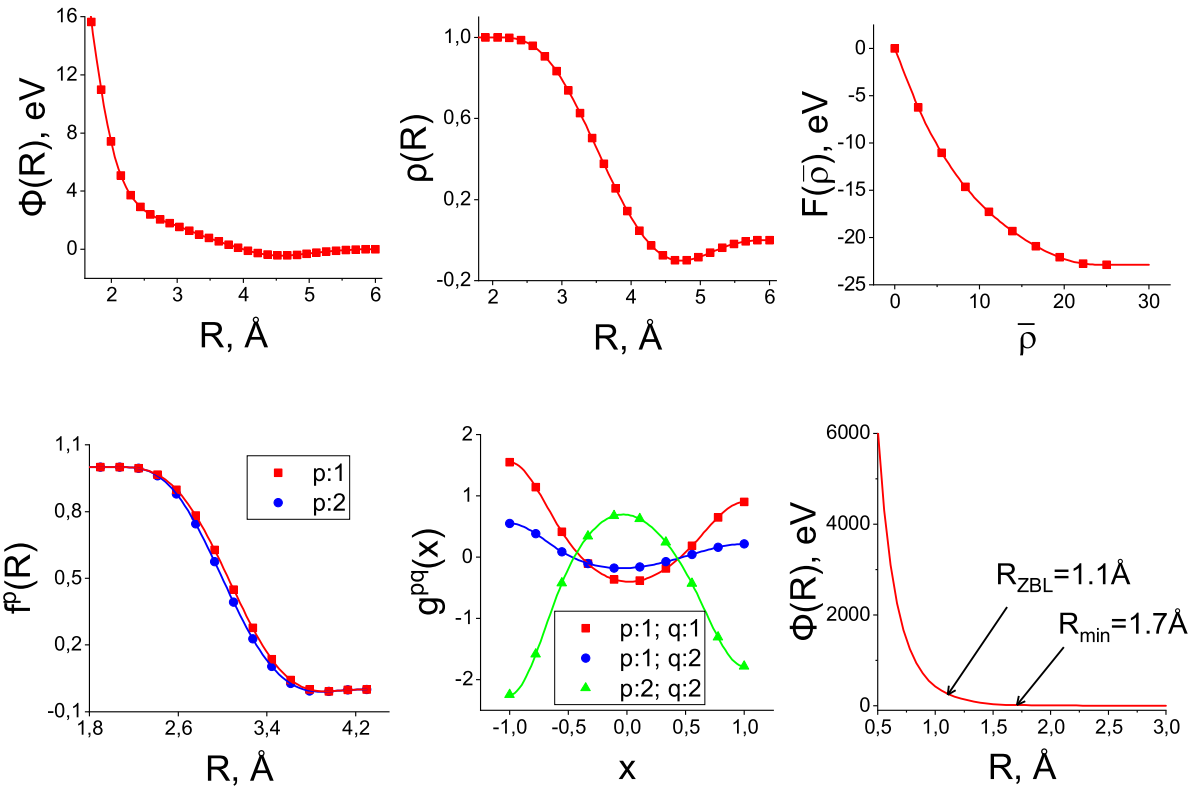

Fig. 1. The potential functions in form of cubic splines describing interactions between W atoms in the POT_W potential. $\Phi(R)$ at $R < R_{ZBL}$ has the form of a Coulomb screened pair potential in Ziegler–Biersack–Littmark (ZBL) form [20] and is a fifth-degree polynomial in $[R_{ZBL}, R_{min}]$.

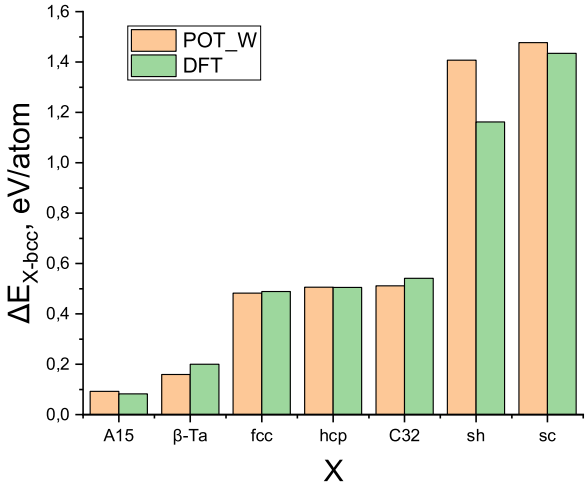

Fig. 2. Energies ΔE_{X-bcc} of a series of model crystal lattices relative to the W bcc lattice equilibrium energy.

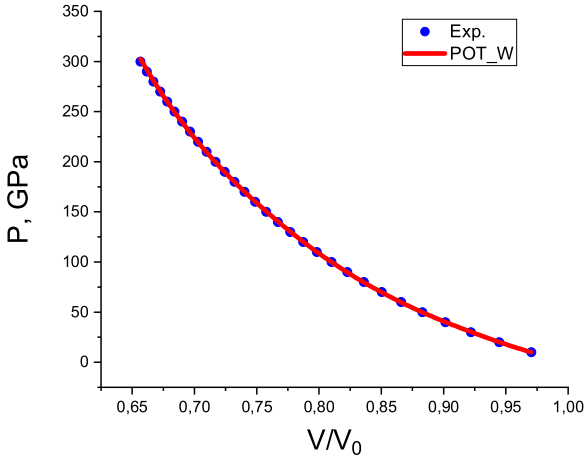

Fig. 3. Pressure (P) - relative volume (V/V_0) dependence for the bcc lattice of W. The experimental values are taken from [25].

the DFT calculations. The maximum deviation from the target values does not exceed 1%, which is obtained for the module C_{44}. At the same time, in contrast to POT_W, the GAP potential [11] shows more significant deviations from the considered experimental values of the W characteristics, reaching 6% in the sublimation energy E_{coh} and 7% in C_{44}, since it was constructed using the DFT fitting database only [11].

As a characteristic of the fitting error of the DFT forces, we used the root-mean-square deviation of the POT_W force vectors from the target DFT force vectors. The DFT values of the force vectors in a superlattice with one atom displaced by 0.05 Å were fitted with an average error of 8% (0.6 meV/Å). In a superlattice at a temperature of 1850 K, the average deviations of POT_W from the corresponding DFT values were 15% (35 meV/Å). For the POT_W force prediction test, we also calculated the POT_W and DFT forces in a 128-atom superlattice with thermal displacements of atoms at a temperature of 3000 K, which was not used to optimize the POT_W potential parameters. The average deviation between the POT_W and DFT forces for this superlattice was 20% (68 meV/Å), which is close to the error of 15% in the case of the superlattice at 1850 K.

Thus, the POT_W potential demonstrates adequate quality of fitting of the target values.

Table 1
Sublimation energy E_{coh}, lattice parameter a_0 at 298 K, and elastic moduli C_{ij} at 0 K for the bcc W. The values of a_0 at 0K are shown in parentheses.

Property	POT_W	Exp.	DFT	GAP[c]
E_{coh}, eV/atom	8.9	8.9[a]	8.39[c]	8.39
a_0, Å	3.165(3.162)	3.165[b]	(3.185)[c]	(3.185)
C_{11}, GPa	525	522[d]	522[c]	526
C_{12}, GPa	204	204[d]	195[c]	200
C_{44}, GPa	163	161[d]	148[c]	149

[a]Ref. [26].
[b]Ref. [27].
[c]Ref. [11].
[d]Ref. [28].

2.3. Simulation software

To test the constructed potential in the reproducibility of the non-fitted quantities, we employed our developed program package for molecular dynamics simulations, which was extensively tested in previous works devoted to the construction of the interatomic potentials for pure V and Ti [8,9], binary potential Ti–V [18], and calculations of diffusivity in Ti–V system [29]. To extend the availability of our interatomic potentials to the broader simulation community, we also implemented them into the LAMMPS package [30]; see Supplementary materials for additional information. In this work, to ensure the reproducibility of results obtained employing our molecular dynamics package with the LAMMPS package, several calculations were performed twice using both packages with the same or similar simulation parameters. The comparison of results is presented in Section 3 and Supplementary materials.

2.4. Testing POT_W

To benchmark the POT_W potential, we calculated the characteristics of vacancy and interstitial atoms, the formation energies of surfaces with low Miller indices, the thermal properties, the phonons dispersion curves and compared them with known experimental data as well as with the results of DFT calculations. Among the selected properties, the melting point represents a key quantity for a reliable quantitative prediction of the characteristics of diffusion processes, along with the monovacancy's properties and the thermal expansion of the lattice. The formation energies of the defects (vacancy, the interstitial atoms, and the surface), as well as the heat of melting, are important test values for a reliable quantitative prediction of the formation of complex crystal lattice defects, including grain boundaries. The reproduction of phonon characteristics in tungsten ensures the mechanical stability of the bcc lattice during MD simulation.

We calculated the characteristics of point defects by molecular statics using a 2000-node bcc superlattice. The surface energy was determined by the molecular static method for slabs as in our previous article[19]. The melting point was calculated by modeling the NPH ensemble [31] in a superlattice containing 19652 atoms, consisting of the equilibrium of the bcc and liquid phases, in the same manner as in our previous works [8,9]. The heat of melting was calculated as the difference in the enthalpy of superlattices containing the liquid and the bcc structure at the determined melting point. We performed MD simulations of thermal expansion in the NPT ensemble (constant number of particles N, pressure P and temperature T) at zero pressure and different temperatures. In the NPT ensemble, temperature was kept constant using Nose–Hoover thermostat [32] and pressure was kept constant using Berendsen barostat [33]. The dispersion curves of the phonons were calculated using the PHONOPY package [34,35] for a 256-atom superlattice.

Table 2
Defect properties of tungsten: E_v^f - vacancy formation energy, E_v^m - vacancy migration energy, Q_v^{diff} - self-diffusion activation energy, $E_{\langle 110\rangle}$, $E_{(100)}$, and $E_{(111)}$ - surface formation energies, $d_{12}(110)$ - relaxation of the distance between the first and second layers, $E^f_{\langle 100\rangle}$, $E^f_{\langle 110\rangle}$, $E^f_{\langle 111\rangle}$, E^f_{oct}, and E^f_{tet}, - interstitial atom formation energies, T_m - melting point, and ΔH_m - melting heat.

Characteristic	POT_W	Exp.	DFT	GAP[g]
E_v^f, eV/atom	3.77	3.67 ± 0.2[a]	3.36, 3.22[g]	3.32
E_v^m, eV/atom	1.81	1.7–1.9[a b]	1.73[h]	1.71
Q_v^{diff}, eV/atom	5.58	5.5[c]	–	5.03
$E_{(110)}$, meV/Å^2	231	187, 203[d]	204[g]	204
			200[i]	
$E_{(100)}$, meV/Å^2	235		245[i]	251
$E_{(111)}$, meV/Å^2	287		216[i]	220
$d_{12}(110)$, %	−1.9	–	−3.8[i]	
$E^f_{\langle 100\rangle}$, eV/atom	10.37	–	12.20[j]	–
$E^f_{\langle 110\rangle}$, eV/atom	10.43	–	10.64[i]	10.55
			10.58[j]	
$E^f_{\langle 111\rangle}$, eV/atom	10.20	–	10.31[i]	10.34
			10.29[j]	
E^f_{oct}, eV/atom	10.21	–	12.42[i]	–
			12.27[j]	
E^f_{tet}, eV/atom	11.03	–	11.72[j]	–
T_m, K	3695 ± 17	3695[e]	3450 ± 100[k]	3540 ± 10
ΔH_m, kJ/mol	40.5	52.3[e]	–	–
		35.4[f]		

[a]Ref. [36].
[b]Ref. [37].
[c]Ref. [38].
[d]Ref. [39].
[e]Ref. [40].
[f]Ref. [41].
[g]Ref. [11].
[h]Ref. [42].
[i]Ref. [43].
[j]Ref. [44].
[k]Ref. [45].

Table 2 shows the results of our calculations of a number of properties of bcc lattice's defects and thermal properties of tungsten determined using the POT_W potential, known experimental measurements, the DFT results, and the recent GAP potential [11]. Among the formation energies of interstitial atoms, we present the values of configurations with the lowest formation energies as they are most important configurations in modeling radiation damage defects. We also present the values of the surface energies among the surfaces with Miller indices (100), (110), and (111).

Table 2 also demonstrates that the values of the vacancy formation energy E_v^f and the vacancy migration energy E_v^m calculated using the POT_W potential are within the range of the experimental values of these quantities. POT_W value of 5.58 eV of the self-diffusion activation energy Q_v^{diff} by the vacancy mechanism is close to the corresponding value of 5.5 eV, established from experimental studies [38]. POT_W value of the surface formation energy (110) is qualitatively consistent with the data of the DFT calculations, according to which this surface has the lowest energy. However, the given by POT_W sequence of (100) and (111) surface formation energies is different from that given by DFT [43] and GAP [11]. The smallest POT_W value of the formation energy of the interstitial atoms is the dumbbell configuration ⟨111⟩ in accordance with the DFT data [43].

It should be noted here that when multiplying the POT_W value of E_v^f=3.77 eV/atom by a factor of 1000, we get a numerical value close to the melting point of tungsten 3695 K. This coincidence is consistent with the empirical rule relating the energy of vacancy formation and the melting point, expressed in eV and K, respectively, which is often true for metals [46]. It is interesting to note that for the DFT values of these quantities in tungsten this rule is also fulfilled. However, the DFT significantly underestimates the values of E_v^f and T_m in W. The POT_W

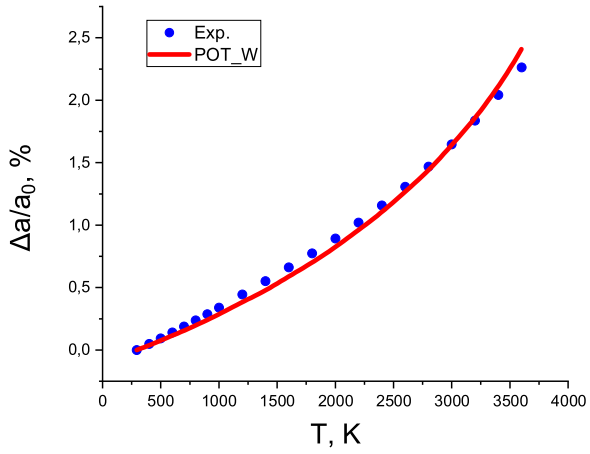

Fig. 4. The dependence of the relative lattice constant on temperature for the bcc tungsten, calculated using the POT_W potential and measured experimentally [47].

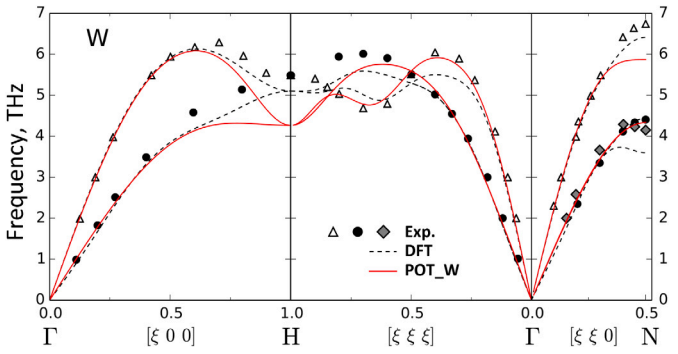

Fig. 5. Dispersion curves of bcc tungsten phonons along the directions of high symmetry of the Brillouin zone for POT_W potential (solid red lines) compared to the experimental data [48] (triangles, circles, rhombuses) and the results of our DFT calculations (dotted lines).

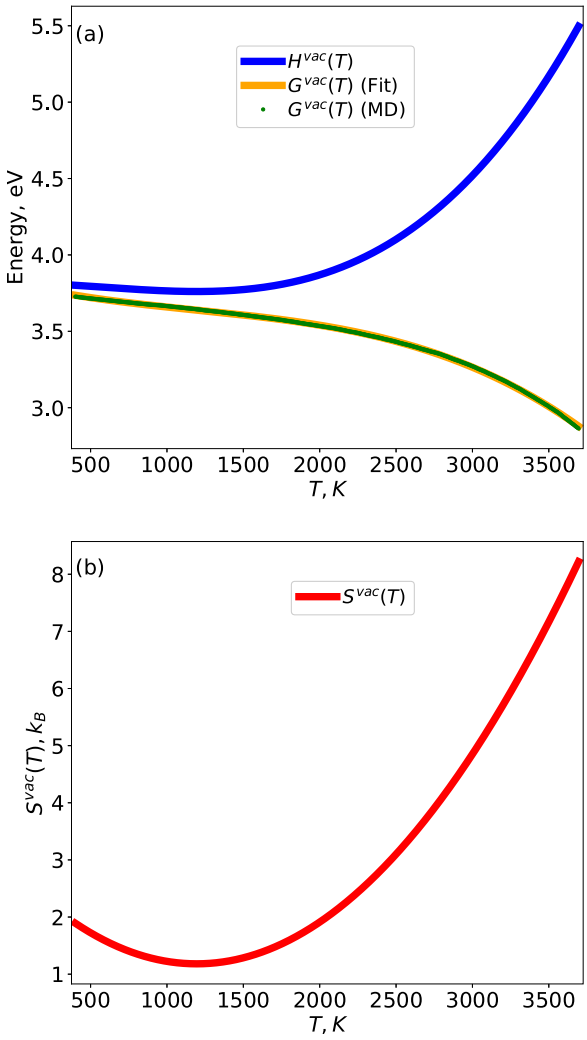

Fig. 6. The vacancy formation Gibbs energy G^{vac}, enthalpy H^{vac} and entropy S^{vac} determined employing Eqs. (6)–(9) for the POT_W potential.

potential predicts the melting point value and thermal expansion of tungsten in perfect agreement with the experimental data [47] as can be seen in Fig. 4. Moreover, the predicted value of the melting heat of 40.5 kJ/mol is consistent with the values of this quantity of 52.3 and 35.4 measured experimentally in [44,45], respectively.

Fig. 5 shows the results of our calculations of the phonon dispersion curves using the POT_W potential and the DFT. The POT_W potential reproduces phonon dispersion for the bcc lattice in close agreement with the experiment [48], especially at low frequencies, which is consistent with the excellent quantitative description of the elastic constants (see Table 1). The POT_W potential predicts the maximum difference from the experimental data at the point H, which is about 1 THz. On the other hand, the POT_W potential shows better agreement with the experiment than the DFT for the wave vectors [$\zeta\zeta\zeta$] between points H and Γ.

In general, as can be seen from the above comparison, the POT_W potential predicts several characteristics of tungsten, including the properties of the vacancy, the interstitial atoms, the surface, the thermal vibrations of the atoms, the melting point and the heat of melting in good agreement with the known experimental data. At the same time, the POT_W potential reproduces the considered values with higher precision than the DFT methods and the interatomic potential, the parameters of which are optimized based on the DFT target values only. The DFT errors are explained by the use of model representations of the exchange–correlation energy functional for the electron subsystem [49], which can be inherited in interatomic potentials. It indicates the advantage of the approach used in the construction of POT_W, based on the simultaneous use of experimental data and a large number of modified DFT values. Meanwhile, it ensures the reliability of the quantitative prediction and the transferability of the potential to configurations not used for optimization.

To test the computational cost of our potential we conducted annealing of the BCC tungsten supercell containing 1999 atoms and one vacancy at a temperature of 650 K for 100 steps with a timestep of 1 fs for the POT_W and GAP [11] potentials employing LAMMPS package. The results demonstrate that our new potential is about 470 times faster than the GAP one. In particular, the computational costs are 16.2 and 7617.8 μs/atom/step for the POT_W and GAP potentials, respectively, on 1 core of Intel Core i7 2670QM processor. For more details please see Supplementary materials, folder Comparison_with_GAP.

3. Self-diffusion in bcc W

We employ the following expression to calculate the diffusion coefficient $D(T)$ in the assumption of the mono-vacancy diffusion mechanism [19]:

$$D(T) = C^{vac}(T) \times N \times D^{vac1}(T). \quad (3)$$

In Eq. (3), $C^{vac}(T)$ is the vacancy concentration at temperature T, N is the number of nodes in the simulation cell, and $D^{vac1}(T)$ is the

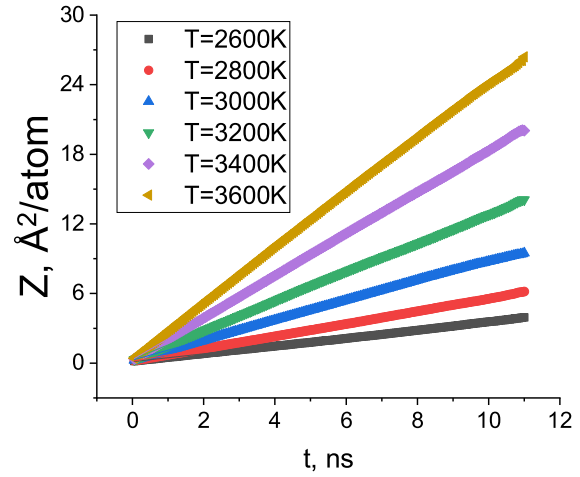

Fig. 7. The mean-squared displacements Z of atoms in a cell of 2000 nodes with one vacancy calculated employing our molecular dynamics package with the POT_W potential.

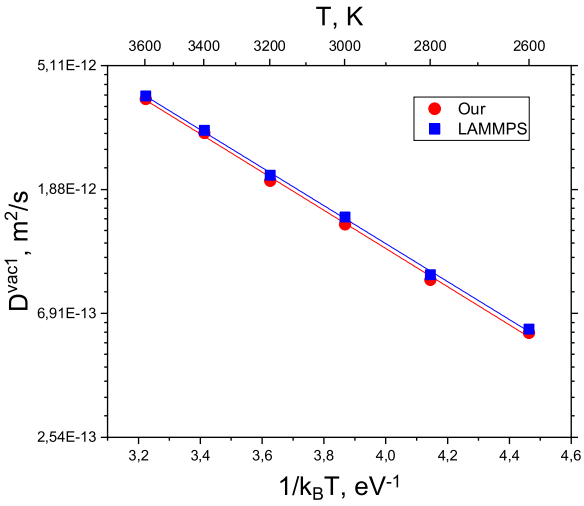

Fig. 8. Dependence of the coefficient D^{vac1} on $1/kT$. The red circles are values obtained from MSD data with our molecular dynamics package, the blue squares are values obtained from MSD data with the LAMMPS [30] package.

diffusion coefficient in a model solid solution containing one vacant node in the simulation cell with periodic boundary conditions.

The vacancy concentration's dependence on temperature is determined as follows:

$$C^{vac}(T) = exp(-G^{vac}(T)/k_B T), \tag{4}$$

where $G^{vac}(T)$ is the Gibbs energy of vacancy formation, which also depends on temperature. To determine these dependencies, we performed calculations using the Gibbs–Helmholtz equation for 432-site bcc supercells with and without the monovacancy.

$$\frac{G^{vac}(T)}{T} = \frac{G_0^{vac}(T_0)}{T_0} - \int_{T_0}^{T} \frac{H^{vac}(T')}{T'^2} dT'. \tag{5}$$

To use this equation we calculated the Gibbs energy $G_0^{vac}(T_0)$ at $T_0 = 400K$ within the quasiharmonic approximation (QHA) and vacancy formation enthalpies at the temperatures 400–3695 K (up to the melting point of W) with temperature step of 5 K. At each temperature, we performed the MD simulations of the NPT ensemble for 100000 steps with a time step of 1 fs. Next, we approximated the obtained from Eq. (5) dependence $G^{vac}(T)$ by the third-order polynomial following the

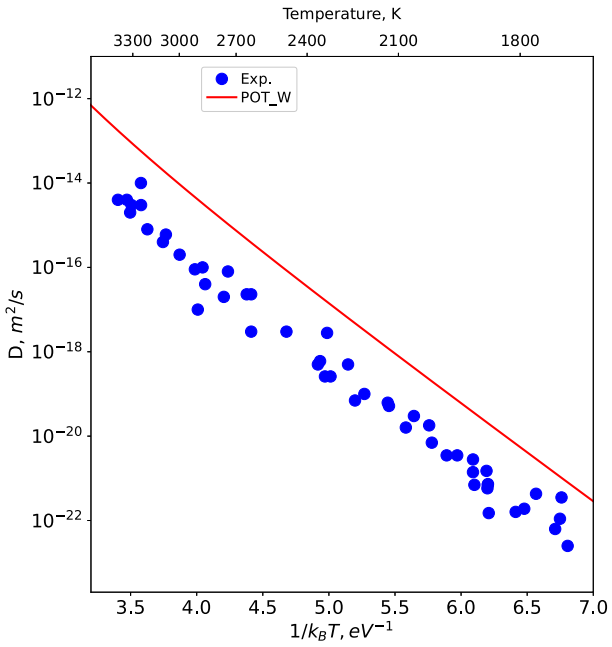

Fig. 9. The self-diffusion coefficient of tungsten $D(T)$ calculated using molecular dynamics package with the POT_W potential and Eq. (12) in comparison with experimental data [50].

Table 3
The coefficients of the polynomial fit of the vacancy formation Gibbs energy $G^{vac}(T)$ for tungsten (Eq. (6)).

g_0, eV	g_1, eV/K	g_2, eV/K^2	g_3, eV/K^3
3.816	-2.40×10^{-4}	1.16×10^{-7}	-3.23×10^{-11}

approach used by Mendelev et al. [5].

$$G^{vac}(T) = g_0 + g_1 T + g_2 T^2 + g_3 T^3 \tag{6}$$

From this expression we determine the vacancy formation enthalpy using the Gibbs–Helmholtz equation

$$\frac{\partial (G^{vac}/T)}{\partial T} = -\frac{H^{vac}}{T^2}, \tag{7}$$

with which we obtain

$$H^{vac} = g_0 - g_2 T^2 - 2 g_3 T^3. \tag{8}$$

Following standard definition $S^{vac} = -\partial G^{vac}/\partial T$, we obtain the expression for the vacancy formation entropy from Eq. (6):

$$S^{vac} = -g_1 - 2 g_2 T - 3 g_3 T^2. \tag{9}$$

The results of calculations of the thermodynamic properties of vacancy employing Eqs. (6)–(9) are presented in Fig. 6 and the polynomial coefficients are listed in Table 3. Fig. 6(a) demonstrates that both formation enthalpy and Gibbs energy of vacancy show the typical behavior as was previously obtained for other metals [4,5]. Meanwhile, Fig. 6(b) demonstrates minimum in the temperature dependence of vacancy formation entropy at about 1250 K. Above this temperature it monotonically rises up to melting point and in the temperature range of diffusion calculations (2600–3600 K) demonstrates the behavior common for metals [4,5,19].

Fig. 7 shows the results of our MD calculations of the mean-squared displacements (MSD) of atoms in a 2000-node bcc supercell containing a single vacant node at six temperatures. For all temperatures, we obtained the linear dependencies of the MSD on simulation time, meaning that the chosen duration of the modeling is enough for obtaining reliable results.

Table A.1
Parameters specifying the eight cubic splines that comprise the potential functions of the POT_W potential. The first part of the table lists the number of knots N for each spline and the range of the spline variables t_{min} and t_{max}. The middle part of the table gives the values at equally spaced spline knots defined by $t_i = t_{min} + (i-1) * (t_{max} - t_{min})/(N-1)$. Finally, the derivatives of the splines at their end points are listed in the last part of the table.

i	t	t_{min}	t_{max}	N				
Φ	r(Å)	1.7	6.0	30				
ρ	r(Å)	1.9	6.0	25				
F	$\bar{\rho}$	0.0	25.0	10				
f^1	r(Å)	1.9	4.3	15				
f^2	r(Å)	1.9	4.3	15				
g^{11}	x	−1.0	1.0	10				
g^{12}	x	−1.0	1.0	10				
g^{22}	x	−1.0	1.0	10				
i	$\Phi(r_i)$ (eV)	$\rho(r_i)$	$F(\bar{\rho}_i)$ (eV)	$f^1(r_i)$	$f^2(r_i)$	$g^{11}(x_i)$	$g^{12}(x_i)$	$g^{22}(x_i)$
1	15.63017304	1.00000000	0.00000000	1.00000000	1.00000000	1.55077134	0.54963086	−2.24892545
2	10.98668821	0.99996621	−6.23422367	0.99988569	0.99986877	1.14078264	0.38077771	−1.58352371
3	7.42141129	0.99790293	−11.04475297	0.99392059	0.99393537	0.41067150	0.08835833	−0.42538250
4	5.08301344	0.98659356	−14.63134878	0.96045782	0.96551597	−0.10673851	−0.10189236	0.34219832
5	3.71678484	0.95776979	−17.29193798	0.87827039	0.89750045	−0.36390915	−0.17786389	0.67170103
6	2.91151065	0.90686541	−19.31836821	0.74485781	0.78271552	−0.38195268	−0.16034392	0.62179521
7	2.40346447	0.83283981	−20.90439604	0.57419213	0.62692610	−0.18667521	−0.07567721	0.24132147
8	2.06293606	0.73765213	−22.09351140	0.39269944	0.44951815	0.18390925	0.04418387	−0.43397397
9	1.79706504	0.62566547	−22.75507302	0.22885639	0.27709192	0.65078238	0.16051734	−1.30950716
10	1.54385618	0.50311988	−22.88165535	0.10364254	0.13593761	0.89961578	0.21438953	−1.78501509
11	1.28229724	0.37710876		0.02663694	0.04333588			
12	1.02272437	0.25467302		−0.00593799	0.00001547			
13	0.77692219	0.14256482		−0.00864271	−0.00755342			
14	0.54310086	0.04709598		−0.00206036	−0.00201214			
15	0.31666731	−0.02659203		0.00000000	0.00000000			
16	0.09936083	−0.07528320						
17	−0.09883858	−0.09861790						
18	−0.26109609	−0.09985999						
19	−0.37274121	−0.08510084						
20	−0.42605892	−0.06219531						
21	−0.42438672	−0.03858040						
22	−0.38079967	−0.01921434						
23	−0.31191627	−0.00658560						
24	−0.23447601	−0.00093271						
25	−0.16106135	0.00000000						
26	−0.09889924							
27	−0.05105292							
28	−0.01861048							
29	−0.00277173							
30	0.00000000							
i	$\Phi'(r)$, (eV/Å)	$\rho'(r)$, (Å^{-1})	$F'(\bar{\rho})$ (eV/Å)	$(f^1)'(r)$ (Å^{-1})	$(f^2)'(r)$ (Å^{-1})	$(g^{11}(x))'$	$(g^{12}(x))'$	$(g^{22}(x))'$
1	−34.95234299	0.0	−0.44556916	0.0	0.0	0.0	0.0	0.0
N	0.0	0.0	0.0	0.0	0.0	0.0	0.0	0.0

Fig. 8 shows the smoothing of data on the MSD of atoms using the Arrhenius dependence,

$$D^{vac1}(T) = D_0 \times exp(-E/k_BT), \tag{10}$$

where D_0 is the pre-exponential factor and E is the activation energy.

As can be seen from Fig. 8, the dependence of D^{vac1} on $1/k_BT$ is linear with a high quality of fitting. The obtained from this dependence activation energy $E = 1.54$ eV is slightly lower than the vacancy migration energy at 0 K (1.81 eV, see Table 2), which can be explained by the influence of thermal fluctuations and thermal expansion. The calculated parameters of this Arrhenius type dependence lead to the following expression of D^{vac1} as a function of temperature.

$$D^{vac1} = (5.56 \pm 0.60) \times 10^{-10} \times exp\left(\frac{-(1.54 \pm 0.03)eV}{k_BT}\right) m^2/s \tag{11}$$

Multiplying the coefficient $D^{vac1}(T)$ (Eq. (11)) with the vacancy concentration $C^{vac}(T)$ (Eq. (4)) according to the formula for $D(T)$ (Eq. (3)) and taking into account the value $N = 2000$, we get the temperature dependence of the self-diffusion coefficient for tungsten, which is illustrated in Fig. 9.

$$D(T) = 1.11 \cdot 10^{-6} \times exp\left(\frac{-(G^{vac}(T) + 1.54)eV}{k_BT}\right) \frac{m^2}{s} \tag{12}$$

As can be seen from the comparison in Fig. 9, the agreement with the experimental data is satisfactory. The performed MD calculations using the POT_W potential are independent from the experimental measurements, and such good reproduction between two methods indicates their reliability. The above-mentioned results prove the accuracy of the POT_W potential for the simulation of the diffusivity processes in tungsten.

4. Conclusions

In this paper, we constructed the interatomic potential for tungsten (POT_W) within the N-body approach that accurately takes into account angular dependence and many-body interactions. This method was previously successfully used to construct the interatomic potentials with the excellent reproduction of thermal properties, such as melting point and thermal expansion, and properties of point defects, which are crucial for the reliable simulation of diffusion properties. The fitting database includes empirical and theoretical data, covering a wide range of different atomic configurations to increase its transferability. The fitted quantities, such as cohesive energy, elastic moduli, the lattice parameter of the bcc structure as well as relative energies between bcc and other commonly known structures, are reproduced in excellent agreement with the target values. Moreover, the potential predicts

quantities not included in the optimization procedure, such as phonon spectra, formation energies of the point defects and surfaces. The POT_W potential demonstrates the ability to describe the bcc lattice parameter in close agreement with the experimental data in a wide temperature range from room temperature up to a melting point, which is necessary for the accurate simulations of diffusion processes. Melting properties coincide with the experimentally measured values within the error of calculations, which means the correct reproduction of the homologous temperature. As a result, the calculation results of self-diffusion in bcc W employing the POT_W potential are in adequate agreement with the experimental points. The temperature dependency of the Gibbs energy of vacancy formation is considered for these calculations. The constructed potential is suitable to calculate the thermodynamic and diffusion characteristics of W and perform simulations involving diffusion processes such as the radiation damage in tungsten.

CRediT authorship contribution statement

V.N. Maksimenko: Writing - original draft, Formal analysis, Investigation. **A.G. Lipnitskii:** Conceptualization, Supervision, Writing - original draft, Methodology, Software. **A.I. Kartamyshev:** Investigation, Writing - original draft, Writing - review & editing, Visualization. **D.O. Poletaev:** Software, Investigation. **Yu. R. Kolobov:** Supervision, Conceptualization.

Declaration of competing interest

The authors declare that they have no known competing financial interests or personal relationships that could have appeared to influence the work reported in this paper.

Data availability

The authors confirm that the data required to reproduce the findings of this study are available within the article and Supplementary materials and can be reproduced by molecular dynamic simulations. The Supplementary materials are available from https://data.mendeley.com/datasets/rn2nr7tjdb.

Acknowledgments

The work was supported by RFBR grant 18-02-00585, by thematic map no. AAAA-A19-119100800130-0 of the Institute of Problems of Chemical Physics Russian Academy of Sciences, and by Ton Duc Thang University. Poletaev D.O. acknowledges the support of the Russian Science Foundation (Grant No. 19-73-00313) under which the implementation of the potential in the LAMMPS package was made. The authors would like to express their sincere thanks to Prof. Dr. Truong Khang Nguyen, Head of Division of Computational Physics, Institute for Computational Science, Ton Duc Thang University, Ho Chi Minh City, Vietnam for giving his value suggestion, comments and support to complete this work as effective.

Appendix A. The cubic splines of W potential

See Table A.1.

References

[1] S.J. Zinkle, A. Möslang, T. Muroga, H. Tanigawa, Multimodal options for materials research to advance the basis for fusion energy in the ITER era, Nucl. Fusion 53 (10) (2013) 104024, http://dx.doi.org/10.1088/0029-5515/53/10/104024.

[2] Y. Chen, Y.H. Li, N. Gao, H.B. Zhou, W. Hu, G.H. Lu, F. Gao, H. Deng, New interatomic potentials of W, Re and W-Re alloy for radiation defects, J. Nucl. Mater. 502 (2018) 141–153, http://dx.doi.org/10.1016/j.jnucmat.2018.01.059.

[3] M.I. Mendelev, B.S. Bokstein, Molecular dynamics study of self-diffusion in Zr, Phil. Mag. 90 (5) (2010) 637–654, http://dx.doi.org/10.1080/14786430903219020.

[4] D. Smirnova, S. Starikov, G.D. Leines, Y. Liang, N. Wang, M.N. Popov, I.A. Abrikosov, D.G. Sangiovanni, R. Drautz, M. Mrovec, Atomistic description of self-diffusion in molybdenum: A comparative theoretical study of non-Arrhenius behavior, Phys. Rev. Mater. 4 (1) (2020) 013605, http://dx.doi.org/10.1103/PhysRevMaterials.4.013605.

[5] M.I. Mendelev, Y. Mishin, Molecular dynamics study of self-diffusion in bcc Fe, Phys. Rev. B 80 (14) (2009) 144111, http://dx.doi.org/10.1103/PhysRevB.80.144111.

[6] N. Gerhard, T. Cornelis, Self-diffusion and impurity diffusion in pure metals: Handbook of experimental data, in: Pergamon Materials Series, Elsevier, Pergamon: Oxford, UK, 2008.

[7] X. Duan, B. Zhou, Y. Wen, R. Chen, H. Zhou, B. Shan, Lattice inversion modified embedded atom method for bcc transition metals, Comput. Mater. Sci. 98 (2015) 417–423, http://dx.doi.org/10.1016/j.commatsci.2014.11.048.

[8] A.G. Lipnitskii, V.N. Saveliev, Development of n-body expansion interatomic potentials and its application for V, Comput. Mater. Sci. 121 (2016) 67–78, http://dx.doi.org/10.1016/j.commatsci.2016.04.008.

[9] A.I. Kartamyshev, A.G. Lipnitskii, V.N. Saveliev, V.N. Maksimenko, I.V. Nelasov, D.O. Poletaev, Development of an interatomic potential for titanium with high predictive accuracy of thermal properties up to melting point, Comput. Mater. Sci. 160 (2019) 30–41, http://dx.doi.org/10.1016/j.commatsci.2018.12.044.

[10] A.G. Lipnitskii, V.N. Maksimenko, I.V. Nelasov, A.I. Kartamyshev, Interatomic potential for the simulation of diffusion processes in tungsten, in: AIP Conference Proceedings, Vol. 2167, AIP Publishing, 2019, 020197, http://dx.doi.org/10.1063/1.5132064.

[11] J. Byggmästar, A. Hamedani, K. Nordlund, F. Djurabekova, Machine-learning interatomic potential for radiation damage and defects in tungsten, Phys. Rev. B 100 (14) (2019) 144105, http://dx.doi.org/10.1103/PhysRevB.100.144105, http://arxiv.org/abs/1908.07330.

[12] W.J. Szlachta, A.P. Bartók, G. Csányi, Accuracy and transferability of Gaussian approximation potential models for tungsten, Phys. Rev. B 90 (10) (2014) 104108, http://dx.doi.org/10.1103/PhysRevB.90.104108.

[13] D.R. Mason, D. Nguyen-Manh, C.S. Becquart, An empirical potential for simulating vacancy clusters in tungsten, J. Phys.: Condens. Matter 29 (50) (2017) 505501, http://dx.doi.org/10.1088/1361-648X/aa9776.

[14] A.O. Boev, A.G. Lipnitskii, I.V. Nelasov, V.N. Saveliev, A.I. Kartamyshev, V.N. Maksimenko, K.P. Zolnikov, Molecular dynamic simulations of the interaction of interstitial atoms with vacancy complexes in v and V-4ti, in: AIP Conference Proceedings, Vol. 1909, (1) AIP Publishing, 2017, 020018, http://dx.doi.org/10.1063/1.5013699.

[15] A. Boev, I. Nelasov, V. Maksimenko, A. Lipnitskii, V. Saveliev, A. Kartamyshev, Molecular dynamics simulations of the excess vacancy evolution in v and V-4ti, in: Defect and Diffusion Forum, Vol. 375, Trans Tech Publ, 2017, pp. 153–166, http://dx.doi.org/10.4028/www.scientific.net/DDF.375.153.

[16] A.O. Boev, K.P. Zolnikov, I.V. Nelasov, A.G. Lipnitskii, Effect of titanium on the primary radiation damage and swelling of vanadium-titanium alloys, Lett. Mater. 8 (3) (2018) 263–267, http://dx.doi.org/10.22226/2410-3535-2018-3-263-267.

[17] A.O. Boev, K.P. Zolnikov, I.V. Nelasov, A.G. Lipnitskii, Molecular dynamics simulation of primary radiation damage in vanadium and alloy V-4Ti, J. Phys.: Conf. Ser. 1147 (1) (2019) 012087, http://dx.doi.org/10.1088/1742-6596/1147/1/012087.

[18] A.I. Kartamyshev, A.G. Lipnitskii, A.O. Boev, I.V. Nelasov, V.N. Maksimenko, D.A. Aksyonov, T.K. Nguyen, Angular dependent interatomic potential for ti–V system for molecular dynamics simulations, Modelling Simulation Mater. Sci. Eng. 28 (5) (2020) 055010, http://dx.doi.org/10.1088/0965-0393/ab8863.

[19] V.N. Maksimenko, A.G. Lipnitskii, V.N. Saveliev, I.V. Nelasov, A.I. Kartamyshev, Prediction of the diffusion characteristics of the V-Cr system by molecular dynamics based on N-body interatomic potentials, Comput. Mater. Sci. 198 (May) (2021) 110648, http://dx.doi.org/10.1016/j.commatsci.2021.110648.

[20] J.F. Zeigler, J.P. Biersack, U. Littmark, The Stopping and Range of Ions in Solids, Vol. 1, Pergamon, New York, 1985.

[21] G. Kresse, J. Furthmüller, Efficient iterative schemes for ab initio total-energy calculations using a plane-wave basis set, Phys. Rev. B 54 (16) (1996) 11169, http://dx.doi.org/10.1103/PhysRevB.54.11169.

[22] P.E. Blöchl, Projector augmented-wave method, Phys. Rev. B 50 (24) (1994) 17953, http://dx.doi.org/10.1103/PhysRevB.50.17953.

[23] J.P. Perdew, K. Burke, M. Ernzerhof, Generalized gradient approximation made simple, Phys. Rev. Lett. 77 (18) (1996) 3865, http://dx.doi.org/10.1103/PhysRevLett.77.3865.

[24] M.P. Methfessel, A.T. Paxton, High-precision sampling for Brillouin-zone integration in metals, Phys. Rev. B 40 (6) (1989) 3616, http://dx.doi.org/10.1103/PhysRevB.40.3616.

[25] R.G. Mcqueen, S.P. Marsh, J.W. Taylor, J.N. Fritz, W.J. Carter, The equation of state of solids from shock wave studies, in: High-Velocity Impact Phenomena, Elsevier, 1970, pp. 293–417, http://dx.doi.org/10.1016/B978-0-12-408950-1.50012-4.

[26] C. Kittel, Introduction to Solid State Physics, seven ed., Wiley, Michigan, 1996, p. 673.
[27] J.S. Shah, M.E. Straumanis, Thermal expansion of tungsten at low temperatures, J. Appl. Phys. 42 (9) (1971) 3288–3289, http://dx.doi.org/10.1063/1.1660727.
[28] G. Simmons, H. Wang, Single Crystal Elastic Constants and Calculated Aggregate Properties, second ed., MIT Press, Cambridge, 1971, p. 370.
[29] A.O. Boev, I.V. Nelasov, A.G. Lipnitskii, A.I. Kartamyshev, D.A. Aksyonov, Self-point defect trapping responsible for radiation swelling reduction in V–Ti alloys, Solid State Commun. 329 (September 2020) (2021) 114252, http://dx.doi.org/10.1016/j.ssc.2021.114252.
[30] S. Plimpton, Fast parallel algorithms for short-range molecular dynamics, J. Comput. Phys. 117 (1) (1995) 1–19, http://dx.doi.org/10.1006/jcph.1995.1039.
[31] H.C. Andersen, Molecular dynamics simulations at constant pressure and/or temperature, J. Chem. Phys. 72 (4) (1980) 2384, http://dx.doi.org/10.1063/1.439486.
[32] S. Nose, A molecular dynamics method for simulations in the canonical ensemble, Mol. Phys. 52 (2) (1984) 255–268, http://dx.doi.org/10.1080/00268978400101201.
[33] H.J.C. Berendsen, J.P.M. Postma, W.F. van Gunsteren, A. DiNola, J.R. Haak, Molecular dynamics with coupling to an external bath, J. Chem. Phys. 81 (8) (1984) 3684, http://dx.doi.org/10.1063/1.448118.
[34] A. Togo, F. Oba, I. Tanaka, First-principles calculations of the ferroelastic transition between rutile-type and CaCl 2-type SiO 2 at high pressures, Phys. Rev. B 78 (13) (2008) 134106, http://dx.doi.org/10.1103/PhysRevB.78.134106.
[35] A. Togo, I. Tanaka, First principles phonon calculations in materials science, Scr. Mater. 108 (2015) 1–5, http://dx.doi.org/10.1016/j.scriptamat.2015.07.021, URL https://doi.org/10.1016/j.scriptamat.2015.07.021.
[36] K.-D. Rasch, R.W. Siegel, H. Schultz, Quenching and recovery investigations of vacancies in tungsten, Phil. Mag. A 41 (1) (1980) 91–117, http://dx.doi.org/10.1080/01418618008241833.
[37] J. Heikinheimo, K. Mizohata, J. Räisänen, T. Ahlgren, P. Jalkanen, A. Lahtinen, N. Catarino, E. Alves, F. Tuomisto, Direct observation of mono-vacancy and self-interstitial recovery in tungsten, APL Mater. 7 (2) (2019) 021103, http://dx.doi.org/10.1063/1.5082150.
[38] E.A. Brandes, G.B. Brook, Smithells Metals Reference Book, Elsevier, Amsterdam, 1992, p. 1800, http://dx.doi.org/10.1016/C2009-0-25363-3.
[39] W.R. Tyson, W.A. Miller, Surface free energies of solid metals: Estimation from liquid surface tension measurements, Surf. Sci. 62 (1) (1977) 267–276, http://dx.doi.org/10.1016/0039-6028(77)90442-3.
[40] A.T. Dinsdale, SGTE data for pure elements, CALPHAD 15 (4) (1991) 317–425, http://dx.doi.org/10.1016/0364-5916(91)90030-N.
[41] D. Lide, CRC Handbook of Chemistry and Physics, 85 ed., CRC Press, Boca Raton [u.a.], 2004, p. 2712.
[42] P.-W. Ma, S.L. Dudarev, Effect of stress on vacancy formation and migration in body-centered-cubic metals, Phys. Rev. Mater. 3 (6) (2019) 063601, http://dx.doi.org/10.1103/PhysRevMaterials.3.063601.
[43] M.R. Fellinger, First principles-based interatomic potentials for modeling the body-centered cubic metals V, Nb, Ta, Mo, and W, (Ph.D. thesis), Ohio State University, 2013, p. 243.
[44] P.-W. Ma, S.L. Dudarev, Universality of point defect structure in body-centered cubic metals, Phys. Rev. Mater. 3 (1) (2019) 013605, http://dx.doi.org/10.1103/PhysRevMaterials.3.013605.
[45] L.G. Wang, A. van de Walle, D. Alfè, Melting temperature of tungsten from two ab initio approaches, Phys. Rev. B 84 (9) (2011) 092102, http://dx.doi.org/10.1103/PhysRevB.84.092102.
[46] Y. Hayashiuchi, T. Hagihara, T. Okada, A new interpretation of proportionality between vacancy formation energy and melting point, Phys. B+C 115 (1) (1982) 67–71, http://dx.doi.org/10.1016/0378-4363(82)90056-0.
[47] Y.S. Touloukian, R.K. Kirby, R.E. Taylor, P.D. Desai, Thermophysical Properties of Matter - the TPRC Data Series. Volume 12. Thermal Expansion Metallic Elements and Alloys, IFI/Plenum, New York, 1975, p. 1442.
[48] C.M.I. Okoye, S. Pal, Lattice dynamics of molybdenum and tungsten, Il Nuovo Cimento D 12 (7) (1990) 941–952, http://dx.doi.org/10.1007/BF02453041.
[49] K. Lejaeghere, V. Van Speybroeck, G. Van Oost, S. Cottenier, Error estimates for solid-state density-functional theory predictions: An overview by means of the ground-state elemental crystals, Crit. Rev. Solid State Mater. Sci. 39 (1) (2014) 1–24, http://dx.doi.org/10.1080/10408436.2013.772503, http://arxiv.org/abs/1204.2733.
[50] J.N. Mundy, S.J. Rothman, N.Q. Lam, H.A. Hoff, L.J. Nowicki, Self-diffusion in tungsten, Phys. Rev. B 18 (12) (1978) 6566, http://dx.doi.org/10.1103/PhysRevB.18.6566.